The Space Interferometry Mission Astrometric Grid Giant-Star Survey. I. Stellar Parameters and Radial Velocity Variability

Dmitry Bizyaev[1,2], Verne V. Smith[1,3], Jose Arenas[4], Doug Geisler[4], Steven R. Majewski[5], Richard J. Patterson[5], Katia Cunha[1,6], Cecilia Del Pardo[7], Nicholas B. Suntzeff[8], Wolfgang Gieren[4]

dmbiz@noao.edu, vsmith@noao.edu, dgeisler@astro-udec.cl, srm4n@virginia.edu, rjp0i@virginia.edu, katia@on.br, cdelpardo@utep.edu, nsuntzeff@noao.edu, wgieren@coma.cfm.udec.cl

ABSTRACT

We present results from a campaign of multiple epoch echelle spectroscopy of relatively faint ($V = 9.5 - 13.5$ mag) red giants observed as potential astrometric grid stars for the Space Interferometry Mission (SIM PlanetQuest). Data are analyzed for 775 stars selected from the Grid Giant Star Survey spanning a wide range of effective temperatures (T_{eff}), gravities and metallicities. The spectra are used to determine these stellar parameters and to monitor radial velocity (RV) variability at the 100 m s^{-1} level. The degree of RV variation measured for 489 stars observed two or more times is explored as a function of the inferred stellar parameters. The percentage of radial velocity unstable stars is found to be very high – about 2/3 of our sample. It is found that the fraction of RV-stable red giants (at the 100 m s^{-1} level) is higher among stars with $T_{eff} \sim 4500$ K, corresponding to the calibration-independent range of infrared colors $0.59 < (J - K_s)_0 < 0.73$. A higher percentage of RV-stable stars is found if the additional constraints of surface gravity and metallicity ranges 2.3 < log g < 3.2 and -0.5 < [Fe/H] < -0.1, respectively, are applied. Selection of stars based on only photometric values of effective temperature ($4300\,K < T_{eff} < 4700\,K$) is a simple and effective way to increase the fraction of RV-stable stars. The optimal selection of RV-stable stars, especially in the case when the Washington photometry is unavailable, can rely effectively on 2MASS colors constraint $0.59 < (J - K_s)_0 < 0.73$. These results have important ramifications for the use of giant stars as astrometric references for the SIM PlanetQuest.

Subject headings: stars: abundances, fundamental parameters, oscillations, late-type — techniques: radial velocities

1. Introduction

The Grid Giant Star Survey (GGSS; Patterson et al. 2001) is a partially-filled, all-sky survey to identify giant stars from $9 \lesssim V \lesssim 17.5$ mag using the Washington $M, T_2 + DDO51$ filter photometric prescription outlined in Majewski et al. (2000). A primary motivation for the survey and a driver of its design is the selection of stars suitable for the Astrometric Grid of the Space In-

[1]National Optical Astronomy Observatory, Tucson, AZ, 85719

[2]Sternberg Astronomical Institute, Moscow, 119899, Russia

[3]McDonald Observatory, University of Texas, Austin, TX 78712

[4]Universidad de Concepcion, Concepcion, Chile

[5]University of Virginia, Dept. of Astronomy, Charlottesville, VA 22903-0818

[6]Observatorio Nacional, Rio de Janeiro, Brazil

[7]University of Texas at El Paso, Dept. of Physics, El Paso, TX 79968

[8]Cerro Tololo InterAmerican Observatory, La Serena, Chile

terferometry Mission (SIM PlanetQuest). These Grid stars, which serve as astrometric references against which the motions of SIM targets are measured, must themselves be as astrometrically stable as possible. Thus, they must be free of stellar or significant planetary companions as well as atmospheric activity (spotting/flaring) that will induce photocenter wobbles at the several microarcsecond level on of order a decade-long timescale (approximately the duration of SIM). G and K giants were selected by the SIM project as the primary stellar constituent of the SIM Astrometric Grid because these stars are the most luminous, common stellar type found in all directions of the sky. High intrinsic luminosity places giant stars at greater distances for a given apparent magnitude, and this increased distance decreases the angular scale of any fixed linear astrometric wobble, thus making these particular stars less likely to be problematical as references. The GGSS project has been undertaken with the specific aim of identifying *subsolar* metallicity giant stars, which are intrinsically more luminous than solar metallicity giants, and also less likely to have planets (see Fischer & Valenti 2005, and references therein).

Despite consideration of such effects for careful selection, all SIM Astrometric Grid candidates require pre-mission monitoring to assess their likelihood of astrometric stability during the mission. One method is to search for variability in other properties, such as brightness and radial velocity (RV). Indeed, we are presently involved, along with other groups, in a large campaign of echelle high-resolution RV monitoring of Astrometric Grid candidates. Fortunately, not all variability in RV (or luminosity) necessarily translates to detrimental astrometric variability. However, some intrinsic photometric and/or RV variability is due to processes that, although benign in terms of photocenter wobble (e.g., radial pulsations), can mask otherwise detectable signatures of problematical sources of variability, like astrometric wobbles due to planetary, brown dwarf or stellar companions. Therefore, because campaigns to monitor radial velocity variability to the precision needed for vetting SIM targets (i.e. $\sim$ 100 m s^{-1}) are both expensive and time consuming, it is useful to understand how intrinsic RV variability of giant stars depends on other stellar properties (like temperature, metallicity, and surface gravity) to optimize efficient selection of giant stars for the Astrometric Grid.

Although it has long been known that stars at the top of the RGB are both brightness and RV-variable (see e.g. Pryor et al. 1988; Cote et al. 1996), there has been little systematic study of this variability as a function of stellar atmospheric parameters, especially at fainter absolute magnitudes. Monitoring of radial velocities for bright red giants has indicated a high probability of their RV variations at the level of 100 m s^{-1} (see Hatzes & Cochran 1994, and references therein). Jorissen et al. (1997) found that red giants with spectral types late G to early K are stable and giants with later spectral types are all variable. At the same time, study of Hipparcos red clump giants (Adelman 2001) reveals photometric stability in this evolutionary phase. Radial velocity jitter at large amplitude is expected for metal-poor, luminous red giants ($M_V \leq$ -1.4) (see Carney et al. 2003).

In their assessment of the suitability of giant stars as SIM Astrometric Grid members, Frink et al. (2001) studied a proxy sample of 86 nearby giant stars selected from the Hipparcos catalogue. Their study included three to eight epochs of high precision (5-8 m s^{-1}) echelle RV measurements on timescales from days to a year. Frink et al. found that most (73 of 84) of the giant stars they investigated have a stable RV at the level of $<$ 100 m s^{-1}, and the peak of the distribution of measured dispersions in velocity occurs at 20 m s^{-1}. However, Frink et al. do report that RV variation is more probable for redder stars ($(B-V) >$ 1.2 in their sample). While the closest match to the survey presented here, the Frink et al. survey contains stars that are much brighter than the expected SIM Grid sample, and, moreover, they did not probe variability as a function of metallicity, which is a key aspect of the stars being found in the GGSS.

Our goal here is to carry out an initial RV-stability assessment of stars more like those expected to fill the Astrometric Grid by focusing on stars taken directly from the GGSS itself. The hope is that RV stability may correlate with some intrinsic stellar property, such as effective temperature, surface gravity, or metallicity. Although the precision of our RV measurements is an order of magnitude less than that of Frink et al.

(2001), it is appropriate for finding RV wobbles at the level needed to identify astrometrically-detrimental grid candidates for the fainter, > 1 kpc distant GGSS candidates (and, indeed, is the precision at which monitoring campaigns of SIM Grid stars are being conducted). Moreover, our sample is almost an order of magnitude larger than that in the Frink et al. survey. The observations studied and discussed here were obtained under an initial JPL-sponsored program in which the internal RV accuracy was set at about 100 m s^{-1}.

2. Observations and Data Reduction

2.1. Sample Selection and Biases

The GGSS finds giant stars by photometry in the Washington $M, T_2 + DDO51$ filters according to the methods described in Majewski et al. (2000). The $(M - T_2, M - DDO51)$ two-color diagram (2CD) effectively distinguishes between late type dwarfs and giants based on the surface-gravity-sensitive Mgb+MgH feature near 5150 Å (where the 130Å –wide DDO51 filter is centered). Photometry was obtained in 1302 evenly placed fields across the celestial sphere, each of area 0.5–1.0 deg^2. The 2CD (i.e., the Mgb+MgH feature) is secondarily sensitive to metallicity and the positions of stars in the 2CD can therefore be used to derive a crude estimate of the metallicity of the likely giant stars. Metal-poor giants are the most widely separated stars in the 2CD from the locus of dwarf stars, and therefore these are the easiest to identify with our methods. Additional details regarding the GGSS can be found in Patterson et al. (2001).

The selection of stars for the present study is biased according to the same specific set of criteria used in the original agreement of the GGSS collaboration with the SIM Project regarding the selection of Astrometric Grid candidates from the GGSS.[1] Giant star candidates are identified from the 2CD and assigned photometric metallicities therefrom. From the apparent magnitude, color and metallicity, an estimate of the absolute magnitude and a photometric parallax distance is assigned (Rhee et al. 2001). For each field, all giant candidates with $V < 13.5$ mag are rank-ordered according to distance, with the most distant star assigned highest priority. The top four ranked stars in each field, yielding more than 4000 candidates of $9.5 \lesssim V \lesssim 13.5$ mag, were passed onto both medium and high resolution spectroscopic observing campaigns (the latter forming the database explored here). Typically, though not exclusively, the most distant giant candidates in each field were also among those with the lowest photometric metallicities brighter than $V = 13.5$ mag. Thus, our spectroscopic sample is biased toward more metal-poor and distant stars than would be found from a random selection of giant stars in the same magnitude range. From the above described sample of more than four thousand stars, we explore here a random subsample of 775 stars in both celestial hemispheres, which constitutes those stars for which multiple high-resolution spectra have been obtained during the first two years of the GGSS follow-up program.

2.2. Spectroscopy

Spectroscopic observations of 434 stars in the northern subsample of GGSS candidates were conducted in the period from January 2001 to December 2002. We made use of the 2.1m telescope at the McDonald Observatory and the Sandiford Cassegrain echelle spectrograph, which provides $R = 55000$ resolution. Th-Ar comparison spectra were taken right before every program star observation. The quality of the data was monitored by observing one or two RV standard stars from Nidever et al. (2002) per night. The adopted setup of the spectrograph enabled us to cover the 5000-5900 Å spectral range and achieve a signal to noise (hereafter S/N) level of order 20-40 in reasonable exposure times (10-30 minutes).

The observed spectra were reduced from two-dimensional to "echelle" format in a standard way with the IRAF[2] software package. Corrections for

[1] In the past year, the SIM Project has modified somewhat the criteria for the selection of stars for the Astrometric Grid, with a focus on stars with magnitudes more typically $V \sim 9 - 11$ mag and chosen from both the GGSS and the Tycho-2 catalogues in a ratio of approximately 1:3. The Tycho stars are selected without foreknowledge of metallicity, and so are expected to be typically near solar metallicity and at smaller distances than stars from the GGSS. In this respect, all of our results are still relevant, however, since the stars included in the present study span the range of properties expected for both GGSS and Tycho-2 stars.

[2] IRAF is distributed by NOAO which is operated by AURA, Inc. under contract with the NSF.

bias, flat field, and scattered light were applied, and cosmic ray hits cleaned out by the IRAF's tasks from *crutil* package. The internal accuracy of the wavelength calibration via the Th-Ar lamp spectra was on average 0.001 Å (and not worse than 0.0018 Å), which corresponds to an RV accuracy of order 55 m s^{-1} (and not worse than 100 m s^{-1}).

Resampling the spectra introduces systematic errors in the wavelength calibration that degrades the RV accuracy. Thus, to preserve the wavelength calibration the spectrum orders were not concatenated to produce a single spectrum, but rather were maintained individually at their natural sampling.

Southern hemisphere GGSS stars were observed with the 1.2-m Swiss telescope and CORALIE velocimeter in 2001-2004 at the ESO La Silla Observatory (Chile), as described by Arenas et al. (2002). CORALIE is an improved version of the ELODIE spectrograph (Baranne et al. 1996). The effective resolution of CORALIE is 50000, it covers the wavelength range 3870 – 6800 Å and it provides a precision of typically 30 m s^{-1} in the radial velocities. Typically a S/N of 10 was achieved for program targets. The radial velocity and its accuracy comes directly from CORALIE's reduction package TACOS (Baranne et al. 1996).

CORALIE provides RVS for 375 program stars directly from the TACOS software. We found that spectra $S/N \leq 4$ have systematically low RV accuracy and rejected them from further analysis. The whole sample of good S/N CORALIE candidates is thus reduced to 341 objects.

While we cannot obtain abundances directly from CORALIE spectra, we incorporate the RVs of these stars in our analysis and adopt photometrically estimated stellar parameters for these stars.

Since the southern sample was observed with a smaller aperture telescope than the northern one, it is biased toward brighter stars: the distribution of the southern V-magnitudes peaks at 11.6 mag whereas the northern sample distribution peak is located at 12.7 mag.

3. Data Analysis

3.1. Radial Velocities

RVs from the McDonald spectra were measured using a cross-correlation methodology with the help of IRAF's *fxcor* task. After the primary reduction the continuum of each order looks almost flat except at its edges where the continuum level looks systematically lower and the S/N is degraded. For the RV analysis we discard the pixels at order edges, which is about $\sim 20\%$ of the total.

Each spectral order was cross-correlated against the RV template separately. The template chosen was the Arcturus spectrum (Hinkle et al. 2000). The cross-correlated pieces of the template spectrum were convolved with a Gaussian corresponding to the FWHM of the Th-Ar lines found for each order. In addition, the corresponding piece of the calibrating Th-Ar spectrum was cross-correlated with a laboratory Th-Ar template (Palmer & Engleman 1983). The Th-Ar template for each order was also convolved with the same Gaussian as for the stellar template in that order. The shift in the radial velocity between the observed Th-Ar and the laboratory reference frame was subtracted from the stellar RV obtained from the cross-correlation via the template. Thus we not only have taken into account the varying instrumental profile by this order-by-order treatment, but we are able to make multiple estimates of the RV for a single observation and thereby assess the errors in our velocities for each star. A few of the spectral orders indicated significantly different RVs from the others because of poor wavelength calibration due to a sparse Th-Ar line sample. We discarded such "bad" orders from our analysis. The remaining orders' radial velocities (RV_i) give us an independent assessment of the mean RV (RV_0) and its accuracy: $RV_0 = \Sigma\ RV_i \cdot w_i\ /\ \Sigma\ w_i$, where w_i is the inverse square of the individual RV error provided by IRAF. The dispersion of this estimate δRV was found as $\delta RV = \sqrt{\Sigma\ w_i \cdot (RV_i - RV_0)^2\ /\ \Sigma\ w_i}$. We show an example of the order-to-order radial velocity difference assessed for the program star G1113+00.20 in Figure 1.

3.2. Stellar Parameters Derived from an Automated Spectroscopic Analysis

In addition to the measured RV's, physical stellar parameters can be derived for the red giants studied here. The effective temperature (T_{eff}) of giant stars can be determined from their broad-band colors. According to an observational calibration given by Alonso et al. (1999), near-infrared colors ($J - K_s$) can be used to estimate T_{eff} for red giants, even with no information on the stellar metallicity and surface gravity. The full release of the All-Sky Point Source Catalog of the Two Micron All-Sky Survey (2MASS) makes available the near-infrared colors of all GGSS candidates. Figure 2 shows the T_{eff} distribution of the combined northern plus southern samples as estimated from ($J-K_s$) colors according to the Alonso et al. prescription. As may be seen, our candidates span a range of temperatures characteristic of red giants. The typical accuracy of 2MASS colors is 0.03 mag in our sample magnitude range. It corresponds to a 100 K accuracy in T_{eff}.

The internal accuracy of the T_{eff} calibration in Alonso et al. (1999) from ($J - K_s$) is of order 125 K. On the other hand, Bessell, Castelli, & Plez (1998) provide a calibration of the $T_{eff}(J - K_s)$ relation for giant stars from NMARCS stellar atmosphere models. The Bessell, Castelli, & Plez results are reproduced by the Alonso et al. data fairly well for typical values of the surface gravity (see Figure 12 in Alonso et al. 1999). The relation from Bessell, Castelli, & Plez (1998) is metallicity-dependent but the difference between stars of [Fe/H]=0.0 and -2.0 (which corresponds to the bulk of our objects, see below) affects T_{eff} by less than 100 K and would not have a significant effect on the applied calibration procedure. From the previous two paragraphs, we expect $\sim$ 160 K accuracy in our derived T_{eff}.

For the northern sample (434 stars) observed at McDonald Observatory, the reduced echelle spectra can be used to determine the surface gravity, $\log g$, and metallicity, [Fe/H], by comparison to a library of synthetic stellar spectra. For this purpose we produced artificial spectra using the MOOG-2002 spectral synthesis package (Sneden 1973). The corresponding stellar models were computed by the ATLAS 9 code (Kurucz 1993). We computed a model set covering the 3800 – 5600 K temperature range, $0.2 \leq \log g \leq 5.6$, and $-3.0 \leq$ [Fe/H] $\leq +0.5$ with steps in these parameters of 200 K, 0.2 dex and 0.2 dex respectively. In all the models we assumed a typical value for the microturbulent velocity of 2 km s^{-1}.

We selected three pieces of spectra to estimate the stellar parameters. The Arcturus spectrum (used as an RV template in §3.1) was split into 40 Å pieces, and the optimal synthetic spectrum's piece and corresponding model parameters were found by least-square fitting. The stellar parameters of Arcturus (obtained by Griffin & Lynas-Gray (1999)) were best reproduced in the regions of 5175 – 5215, 5215 – 5255, and 5700 – 5740 Å. These wavelength intervals used to derive the stellar parameters are not simply dominated by Fe absorption lines, but also by (principally) lines of Mg I, Ti I, Cr I, Ni I, and to a lesser degree V I. The abundances derived in this way are therefore not direct "Fe abundances", but an overall "metallicity" defined by a mixture of both Fe-peak and α elements; we refer to this abundance as simply metallicity and denote it in the remainder of this paper as [Fe/H]. Although significantly non-solar abundance ratios, relative to Fe, could create additional noise in the metallicity estimates, the vast majority of stars in the sample are well above [Fe/H] $\sim$ -2. Within this metallicity regime only Mg/Fe, and to a lesser extent Ti/Fe and Cr/Fe, are mildly non-solar and typically enhanced. This may introduce a small trend of slightly larger derived overall metallicities as the Fe abundance decreases.

To match the wavelength intervals defined above, spectra of program stars were corrected to zero radial velocity incorporating the RVs defined in § 3.1. The continuum level in the fragments of spectra was fit by a linear function using the *continuum* task from the IRAF package. The pieces of synthetic spectra utilized for the comparison were convolved with a Gaussian corresponding to the FWHM of each echelle order to reduce their spectral resolution to that in the observed data. Then we find the best-fit model for each piece by the least-square method. The values and errors of log g and [Fe/H] were finally obtained by averaging these same derived parameters across the set of three modeled pieces.

With this method, we derived the stellar parameters (T_{eff}, *log g*, [Fe/H]) for the 434 north-

ern GGSS stars (see Table 1). The [Fe/H] for the whole GGSS sample has also been estimated photometrically (Rhee et al. 2001)[3] and one can compare the values derived by each method (photometric and spectroscopic). Figure 3 shows that the two [Fe/H] estimates for most stars of intermediate metallicity ([Fe/H] = -1.0 to 0.0) follows a linear relation with dispersion of the order of 0.4 dex, but systematically offset by 0.16 dex (in the sense that the spectroscopic metallicities tend to be larger). This small offset could be due partially to mildly elevated Mg/Fe, Ti/Fe, or Cr/Fe ratios in the metal poor stars. There are some extreme outliers in Figure 3. Some of these stars have large error bars, either in their spectroscopic or photometric metallicities. Many of the outlying points in Figure 3 correspond to the hottest stars in our sample. These stars occupy the border region between giants and dwarfs on the giant-dwarf discrimination diagram from Majewski et al. (2000), and their stellar parameters determined from photometric data may be biased.

Figure 4 shows the relation between the surface gravity and effective temperature for the northern hemisphere sample. Most of the stars in Figure 4 span ranges typical for red giants. Here we see the success rate of the GGSS for photometrically identifying bona fide red giants to be extremely high: more than 98 % of the stars that were photometrically identified by the Majewski et al. (2000) method to be giant stars have spectroscopic gravities supporting this characterization.

3.3. Errors in Atmospheric Parameters

In order to analyze the accuracy of the derived stellar parameters as a function of the quality of observed spectra, we performed Monte Carlo simulations deriving the basic stellar parameters for a set of selected synthetic spectra deteriorated by varying amounts of added noise. We considered a set of signal-to-noise ratios from 3 to 30 which covers the typical range of S/N in our observed spectra. Besides random noise, we also added variations of T_{eff} and RV into the model spectra, distributing them uniformly within $\pm$100 K and $\pm$100 m s^{-1} range from the true value. Finally, we assumed that the microturbulence velocity might take an arbitrary value in the range 1 to 2 km s^{-1}. The stellar parameters were defined for a hundred resulting synthetic spectra over the typical (see Figure 4) values of T_{eff} and $log\ g$: (4000 K and 1.4 dex), (4400 K and 2.6 dex), and (5000 K and 3.0 dex). The [Fe/H] took the values -2, -1, and 0 dex for each case. The resulting ranges of the estimated parameters (1-$sigma$ level) are shown by the solid curves in Figure 5 about the mean values (designated by the diamonds). The dashed lines represent the initial true parameters (log g or [Fe/H]) of the spectra. The figure shows that we obtain an accuracy in log g of the order of 0.2 dex. A systematic difference in log g of +0.1 dex is found and is primarily the result of the displacement of the microturbulent velocity ξ from the adopted 2 km s^{-1}. The metallicity is defined with 0.1 dex accuracy and a possible displacement of all estimated values (again due to the unknown ξ) is -0.05 dex. To check if these results depend on the number of Monte Carlo simulations, we also evaluated some models based on sets of 400 deteriorated spectra instead of 100. No obvious differences can be seen compared with the case of 100 simulations.

We also extend the considered S/N ratio up to 100. High values of S/N do not improve the inferred parameters since the ξ uncertainty introduces the most significant error. The next strongest factor introducing a systematic deviation between the "real" and estimated stellar parameters is the RV error. It is seen that starting with $S/N = 10$ and better one can estimate surface gravity and metallicity from our spectra with quite good accuracy. Most of our spectra in the northern sample satisfy this criterion. Note that the accuracy of the RVs also depend on S/N. This can be a reason for more significant errors in log g and [Fe/H] obtained from our spectra.

3.4. Stellar Parameters Derived from a Classical Spectroscopic Analysis

Some of the higher S/N spectra from GGSS stars studied here are suitable for a detailed abundance analysis from which stellar parameters and iron abundances can be obtained via measurements of individual equivalent widths from a selected sample of Fe I and Fe II lines. This is a different technique from the straightforward match-

[3]These photometrically derived metallicities are those that have been delivered by the GGSS collaboration to the SIM project.

ing of observed and synthetic spectra used in Section 3.2, which we will refer to as the "automated spectroscopic" method. When a strictly spectroscopic method (using a line-by-line analysis) is adopted, the effective temperatures can be obtained by forcing a zero slope in the relation between Fe I abundances with line excitation potentials; surface gravities are obtained from the agreement between the abundances from Fe I and Fe II lines. Another parameter that can be adjusted at the same time is the microturbulence velocity, which is tuned so that the Fe I abundances are independent of the equivalent widths.

This method can provide a consistency check on the metallicities and *log g* derived with the automated method presented in Section 3.2. To test the degree of consistency, a small sub-sample of 10 target stars, with larger than average S/N values, were selected as candidates for the detailed spectroscopic analysis. Our approach consisted of adopting the same effective temperatures from the Alonso et al. (1999) photometric calibration for the target stars and to use a sample of Fe I and Fe II lines that were tested to produce good results for the Sun, as well as the well-studied red-giant Arcturus. The sampled Fe lines and their atomic parameters are listed in Table 2: for each transition the excitation potential and gf-value are listed. The equivalent-width measurements are presented in Table 3. The same spectrum analysis code MOOG was used in the abundance computations based on the individual equivalent-width measurements. The adopted effective temperatures, and derived surface gravities, microturbulent velocities, and iron abundances are presented in Table 4. A comparison of surface gravities derived using the Fe I and Fe II lines with those obtained from the automated method finds a systematic mean offset of [log g(automated) - log g(Fe I/Fe II)]= +0.4±0.4 dex. As the Fe II lines are quite sensitive to stellar surface gravity, this systematic offset may suggest that the surface gravities derived from our automated method are somewhat overestimated.

The derived Fe abundances from this detailed analysis are intercompared in Figure 6 with the metallicities obtained from Washington + DDO51 photometry (upper panel) and automated spectroscopy (middle panel). The metallicity distributions shown in the middle and lower panels of the figure are in generally good agreement, with the same standard deviation of 0.18 dex, but an an offset of 0.18 dex in the average [Fe/H]. Such an offset is within the quoted uncertainties in the metallicities obtained from the automated method (of roughly 0.2 to 0.3 dex). Moreover, because the automated method does not measure a true Fe abundance, but an overall general metallicity affected by a mixture of elements, a mild offset between the two methods is not unexpected.

An important aspect of this additional verification of the results obtained with the automated method is a check on the derived surface gravities using Fe I and Fe II lines directly, via ionization equilibrium. As discussed previously, the GGSS targets were selected from Washington photometry two-color diagrams to be giant stars and not dwarfs. The values of log g derived for this subsample of stars, as can be seen in Table 4, confirms their evolved status as red giants. Both the direct analysis of Fe I and Fe II ionization equilibrium, as well as the automated direct comparison with model spectra, indicate that the Washington + DDO51 two-color diagram is an effective method for identifying red giants.

4. RV Stability Versus Stellar Parameters

We now focus on the 148 stars of the northern sample whose RVs were measured two or more times with large epoch differences (a time between successive observations of the same star not less than 4 months). From these data we estimate the RV dispersion which we designate as σ and utilize this as a measure of variability of the RV. Note, this is not the statistical standard deviation widely designated by σ; the present σ is calculated from multiple RV measures after weighting each by the inverse square of the accuracy of each RV measure (w_j): $RV_m = \Sigma\ RV_j \cdot w_j\ /\ \Sigma\ w_j$, and

$$\sigma = \sqrt{\Sigma\ w_j \cdot (RV_j - RV_m)^2\ /\ \Sigma\ w_j}. \quad (1)$$

Here w_j is the weight. If the accuracy of the corresponding RV was better than 50 m s^{-1}, we assume it equals 50 m s^{-1} because of the wavelength calibration uncertainty (see §3.2).

The derived values of σ are shown in Table 5. Figure 7 (upper panel) shows the distribution of the σ values (in km s^{-1}). The largest number of sources occur in the first bin reveals the accuracy

of our estimates and confirms that its value is of the order of 50 m s^{-1}, as it follows from the accuracy of the wavelength calibration (section §2.2).

We next incorporate the repeated RV data obtained with CORALIE for the southern GGSS subsample (Arenas et al. 2002) in Figure 7 (lower panel) with 341 stars in this sample (see Table 6). Variation of the radial velocity σ for the southern stars observed two and more times is estimated by Equation (1). A gaussian curve corresponding to 100 m s^{-1} sigma is shown in Figure 7 by dashed line. Both southern and northern subsamples exhibit similar behavior in their respective RV-variability distributions.

We found no large, apparent systematic difference in the stellar parameters between the RV-stable (low σ) and unstable (high σ) fractions of the sample. However, for stars with $\sigma < 100$ m s^{-1} the *ranges* of the stellar parameters appear to be narrower than for red giants with $\sigma > 100$ m s^{-1}. Thus, the fraction of RV-stable stars is low among very cool ($T_{eff} < 4000$ K) as well as metal-poor stars with [Fe/H] < -1.0, in agreement with previous conclusions by Jorissen et al. (1997) and Carney et al. (2003).

The fraction of RV-stable and unstable stars can be estimated from the distributions of T_{eff}, $log\ g$, [Fe/H], and absolute magnitude M_V presented in the left-hand panels of Figure 8; here the distributions of stars with $\sigma < 100$ m s^{-1} (dashed lines) are shown in comparison with the distributions for all stars (dotted lines). An assessment of M_V is made with T_{eff}, $log\ g$, and an assumption of fixed mass for the red giants (we assume it equals to 0.9 $M_\odot$; variation of the mass introduces insignificant scatter in M_V). The right-hand panels of Figure 8 show the fraction of stable stars in each bin of the histograms shown on the left. As seen in the figure, the fraction of stable stars has a peak in the range 4300-4700 K (secondary peaks at the wings of the distribution are caused by small number statistics). Note that this range corresponds to the extinction-corrected $(J-K)_0$ values from 0.59 to 0.73 mag, and these values do not depend on the choice of color-temperature calibration. Figure 2 shows that the bulk of the giant stars selected from the GGSS Washington+$DDO51$ photometry survey occupies this range of temperatures, showing that the GGSS happens to be optimized for selecting stars in the most RV-stable temperature range.

A similar peak takes place at log $g = 2.3 - 3.2$ in the surface gravity distribution. We also find that the largest fraction of RV-stable stars happens for stars of slightly subsolar metallicity (-0.5 ≤ [Fe/H] ≤ -0.1), and then the fraction of stable stars appears to drop precipitously near solar metallicity. Note, however, that the latter conclusion needs for an additional check since the most metal rich bin is only sampled by 6 stars.

An analog of Figure 8 is drawn for the southern subsample in Figure 9. Here we use the "photometric" [Fe/H] derived by Rhee et al. (2001). The surface gravity is established by way of interpolation of the isochrones published by Bergbusch & Vandenberg (1992). The histograms for T_{eff} defined by the same method for both subsamples of northern and southern stars, are qualitatively similar in Figures 8 and 9. Though the other parameters are estimated by different ways, the corresponding histograms for [Fe/H], log g, and M_V are qualitatively rather similar.

In order to better constrain what types of stars may be most RV-variable we again focus on the McDonald data and the stellar parameters derived from these spectra. In Figure 10 the values of log g are plotted versus the effective temperatures: this is a spectroscopic version of an HR-diagram. The top panel contains those stars with RV variability of less than 100 m s^{-1}, while the bottom panel are the definite RV variables having $\sigma > 100$ m s^{-1}. Superimposed on these stellar points are isochrone curves from Girardi et al. (2000); two metallicity isochrones are shown (the solid curves have [Fe/H]=0.0 while the dashed curves have [Fe/H]=-0.7) with two ages for each metallicity (3.5 and 8.9 Gyr). Plotted this way, the initial RV-results indicate that those stars exhibiting variability of less than ∼100 m s^{-1} tend to be more concentrated in the $log\ g - T_{eff}$ plane, near the He-core burning clump for near-solar metallicities. The stars tending to show RV-variability fall all along either well-defined first-ascent RGB, or AGB, both at somewhat low metallicities. Given uncertainties in both the models and the gravities and temperatures derived by us (which almost certainly also carry some systematic differences), the concentration of possibly RV-stable red giants near T_{eff}∼4500K and log g ∼2.5-3.0 coincides quite closely to the red giant clump for stars having metallicities near solar,

or slightly lower. Note that real log g may have systematically lower values than those shown in Figure 10 (see also §3.4).

The possible association of quasi-RV stability with the red giant clump can be investigated further by including the southern sample, although we do not have spectroscopically derived gravities for these stars. For a relatively old population, however, the effective temperature of the clump does not vary much if the metallicity does not vary by much: this can been seen by inspecting the isochrones in Figure 10. The indications from the McDonald results are that the RV-stable red giants are only mildly metal poor with a relatively small dispersion in metallicity. For the 36 McDonald RV-stable stars having T_{eff}=4500±200K (corresponding to the observed "clump" of points in Figure 10), the mean metallicity is [Fe/H]=-0.5±0.2. The combined northern and southern samples are plotted as effective temperature histograms in Figure 11, where the sample has been segregated using σ. There is a clearly defined clump of potentially RV-stable stars with T_{eff}∼4500K that probably corresponds to core-He burning red giants with mild metal deficiencies. The stars with σ >100 m s^{-1}, shown in the bottom panel, are significantly more dispersed in T_{eff}, with almost equal numbers over a range in effective temperature; our suggestion is that these are primarily first-ascent giants or AGB stars, as well as intrinsically RV-stable stars (such as clump giants) that have companions. The fraction of stars whose RV-variability is caused by components is not known from our observations. Demonstrating the presence of companions will require much more repeated observations.

Preliminary results from monitoring of photometric variability of a subsample of GGSS stars by Bizyaev et al. (2004) reveal no correlation between RV- and brightness variations. However, more precise and *simultaneous* photometric and spectroscopic observations are needed to shed light on the nature of the RV variations in red giants.

4.1. Strategies for Selecting SIM Astrometric Grid Stars

Our analysis gives insight into the optimal selection of giant stars for the SIM Astrometric Grid if time and resources are limited (as indeed they are) for ground-based vetting of large numbers of stars for the most RV-stable specimens.

As can be seen in Figure 11, a higher fraction of stars with σ < 100 m s^{-1} can be found with $4300\,K < T_{eff} < 4700\,K$. This is a simple, straightforward selection criterion resulting in an initial success rate of 50% in finding RV-stable red giants. As a point of reference, the entire northern sample contains 39% stable stars and the southern sample contains 32%. If high-resolution spectra are also used to derive surface gravities and metallicities, the additional constraints of -0.5 < [Fe/H] < -0.1, and $2.3 < log\ g < 3.2$ lead to a 81% and 40% success rate for the northern and southern samples, respectively, yet significantly narrows the sample. Note that the northern sample restricted simultaneously by all stellar parameters reveals the fraction of RV-stable stars that is close to findings by Frink et al. (2001).

More attention to exploring the solar and higher metallicity ranges is warranted because if the relatively low RV-stable fraction we find at these solar-like metallicities is borne out it would have serious ramifications for the currently selected SIM Astrometric Grid sample, which is dominated by giant stars randomly selected from the Tycho catalogue. Spectroscopic metallicities measured for nearly 500 Tycho giants by J. Crane (in preparation) in the preferred magnitude range ($V < 11$) for the SIM Grid stars indicates a median metallicity for this sample of [Fe/H] = -0.1, and perhaps larger (i.e., 0.0 dex) if the arguments for the need of a +0.1 dex correction to the local metallicity scale are applied (Reid 2002; Haywood 2002). Thus, a significant fraction of the Tycho sample is at metallicities where a large fraction of stars may have troublesome atmospheric jitter.

5. Conclusions

We are carrying out high-resolution spectroscopic observations of an all-sky sample of giants which was pre-selected based on the GGSS program of Washington photometry. The GGSS was intended to identify stars with the highest likelihood of astrometric stability — namely, subsolar metallicity red giants. The main purpose of the present study is to make an initial assessment of the RV-variability properties of GGSS stars as a function of their atmospheric characteristics. The RV variation was estimated for 489

stars with spectroscopy taken on both Northern and Southern telescopes. Basic stellar parameters were estimated for the northern subsample from high-resolution spectroscopy.

A surprisingly high fraction of investigated giant stars have unstable radial velocities at 100 m s^{-1} level: about 2/3 of our sample. Both of the samples, northern and southern, although having been observed independently and with different instruments and techniques, show similar distributions of RV variability. Although a number of obvious spectroscopic binaries are included in this sample, much of the low-amplitude RV variability is probably due to atmospheric motions and temperature inhomogeneities.

A higher fraction of stars with $\sigma < 100$ m s^{-1} can be found among the objects with $4300\,K < T_{eff} < 4700\,K$, which corresponds to $(J-K)_0 = 0.59 - 0.73$. If we incorporate spectroscopic metallicity and surface gravity information as well, and select only stars with -0.5 < [Fe/H] < -0.1 and 2.3 < log g < 3.2, it will help to identify RV-stable candidates more effectively, but narrows the sample of potential candidates substantially. From the point of view of minimizing expensive observations, the optimal way of preliminarily selecting RV-stable stars is to use the effective temperature, or more exactly, the calibration independent range of NIR colors as $0.59 < (J-K)_0 < 0.73$. This range encompasses 44% of stars with $\sigma < 100\,m\,s^{-1}$ in both our southern and northern samples; 38.5% of the initial GGSS sample of candidate Astrometric Grid stars (1710 of 4440) lies in this range. The result obtained here will aid in the continuing efforts to define the astrometric reference grid for SIM.

The GGSS follow-up observations presented here have been supported by the JPL and NASA via grant 99-04-OSS-058. The photometric portion of the GGSS was funded by NASA/JPL grants 1201670 and 1222563 to SRM and RJP, and with substantial contributions of additional funding from a David and Lucile Packard Foundation Fellowship to SRM. VVS acknowledges support for part of this work from NASA via grant NAG5-13175. We are grateful to the staff of McDonald observatory for their help and support of both photometric and high resolution spectroscopic observations, and from the Carnegie Observatories for similarly generous contributions for photometric and medium resolution spectroscopic observations of the GGSS. This publication makes use of data products from the Two Micron All Sky Survey, which is a joint project of the University of Massachusetts and the IPAC/Caltech, funded by the NASA and NSF.

REFERENCES

Adelman, S., Baltic Astronomy 2001, 10, 593

Alonso, A., Arribas, S., Martinez-Roger, C. 1999, A&AS, 140, 261

Arenas, J., Geisler, D., Majewski, S., Smith, V. et al. 2002 AAS, 201, 115.05

Baranne, A., Queloz, D., Mayor, M. et al. 1996, A&AS, 119, 373

Bergbusch, P., Vandenberg, D. 1992, ApJS, 81, 163

Bessell, M., Castelli, F., Plez, B. 1998, A&A, 333, 231

Bizyaev, D., Smith, V. V., Arenas, J., Geisler, D. 2004, AAS, 205, 91.07

Carney, B., Latham, D., Stefanik, R. et al. 2003, AJ, 125, 293

Cote, P., Pryor, C., McClure, R. D., Fletcher, J. M., & Hesser, J. E. 1996, AJ, 112, 574

Fischer, D., Valenti, J. 2005, ApJ, 622, 1102

Frink, S., Quirrenbach, A., Fischer, D., Röser, S., & Schilbach, E. 2001, PASP, 113, 173

Girardi, L., Mermilliod, J.-C., & Carraro, G. 2000, A&AS, 141, 371

Griffin, R., Lynas-Gray, A. 1999, AJ, 117, 2998

Hatzes, A., Cochran, W. ApJ1994, 432, 763

Haywood, M. 2002 ,MNRAS, 337, 151

Hinkle, K., Wallace, L., Valenti, J., & Harmer, D. Visible and Near Infrared Atlas of the Arcturus Spectrum, 3727-9300 Å 2000, (San Francisco: ASP) ISBN: 1-58381-037-4

Jorissen, A., Mowlavi, N., Sterken, C., Manfroid, J. A&A1997, 324, 578

Kurucz, R. L. 1993, CD-ROM, Cambridge, MA: Smithsonian Astrophysical Observatory, December 4, 1993

Majewski, S. R., Ostheimer, J. C., Kunkel, W. E., & Patterson, R. J. 2000, AJ, 120, 2550

Nidever, D. L., Marcy, G.W., Butler, R.P., Fischer, D.A., Vogt, S.S. 2002, ApJS, 141, 503

Palmer, B. A., Engleman, R., Jr. 1983, Atlas of the Thorium Spectrum, Los Alamos National Laboratory, Los Alamos, New Mexico

Patterson, R. J., Majewski, S. R., Slesnick, C. L., et al. Small Telescope Astronomy on Global Scales, ASP Conf. Ser. v.246, IAU Colloquium 183. Ed. by Bohdan Paczynski, Wen-Ping Chen, and Claudia Lemme. San Francisco: Astronomical Society of the Pacific, 2001, p.65

Pryor, C. P., Latham, D. W., & Hazen, M. L. 1988, AJ, 96, 123

Reid, I. N. 2002, PASP, 114, 306

Rhee, J., Slesnick, C., Crane, J., Polak, A. et al. 2001 AAS 198, 62.03

Sneden, C. 1973 Ph.D. thesis, Univ. of Texas, Austin

This 2-column preprint was prepared with the AAS LaTeX macros v5.2.

TABLE 1

STELLAR PARAMETERS FOR THE ENTIRE MCDONALD SAMPLE OF 434 GGSS STARS.

Name	RA (J2000.0) (HH:MM:SS)	DEC (J2000.0) (DD:MM:SS)	T_{eff} K	$[Fe/H]_{ph}$ (dex)	D_{ph} (Kpc)	log g_{sp} (dex)	Δ log g_{sp} (dex)	$[Fe/H]_{sp}$ (dex)	$\Delta[Fe/H]_{sp}$ (dex)
G2358+00.31	00:00:51.96	00:22:16.8	4290	-0.3	1.3	4.87	0.19	-2.80	0.05
G2358+00.92	00:01:36.38	00:14:09.9	4399	-0.9	1.1	2.24	0.13	-0.42	0.05
G0001+00.94	00:04:20.08	00:27:12.2	4324	-0.7	3.0	2.67	0.41	-0.40	0.16
G0011+05.87	00:14:18.85	05:57:37.5	4440	-0.5	0.7	2.13	0.19	-0.47	0.09
G0011+16.75	00:14:26.65	17:16:03.0	4594	-0.8	1.8	1.47	0.38	-0.67	0.19
...									

NOTE.—Name of star, its RA and DEC, effective temperature, photometric metallicity [Fe/H], photometric distance, spectroscopic surface gravity log g and its accuracy, and spectroscopic metallicity and its accuracy.
The full version of the Table is presented in electronic form.

TABLE 2
THE FE I & FE II LINES

$\lambda(\AA)$	Species	χ(eV)	$\log gf$
5307.361	Fe I	1.608	-2.970
5322.041	Fe I	2.279	-2.840
5497.516	Fe I	1.011	-2.840
5501.464	Fe I	0.958	-2.957
5522.447	Fe I	4.209	-1.400
5536.583	Fe I	2.832	-3.812
5539.284	Fe I	3.642	-2.660
5549.948	Fe I	3.695	-2.904
5559.638	Fe I	4.988	-1.829
5560.207	Fe I	4.435	-1.040
5577.031	Fe I	5.033	-1.551
5579.335	Fe I	4.231	-2.406
5607.664	Fe I	4.154	-2.258
5608.974	Fe I	4.209	-2.402
5611.361	Fe I	3.635	-2.993
5618.631	Fe I	4.209	-1.260
5619.224	Fe I	3.695	-3.256
5636.696	Fe I	3.640	-2.608
5638.262	Fe I	4.220	-0.720
5661.012	Fe I	4.580	-2.432
5677.684	Fe I	4.103	-2.694
5679.025	Fe I	4.652	-0.770
5696.103	Fe I	4.549	-1.997
5698.023	Fe I	3.640	-2.689
5705.466	Fe I	4.301	-1.360
5717.835	Fe I	4.284	-0.980
5724.454	Fe I	4.284	-2.627
5759.261	Fe I	4.652	-2.073
5760.345	Fe I	3.642	-2.490
5784.657	Fe I	3.397	-2.673
5793.913	Fe I	4.220	-1.697
5806.717	Fe I	4.608	-0.900
5807.782	Fe I	3.292	-3.404
5809.217	Fe I	3.884	-1.690
5811.917	Fe I	4.143	-2.427
5814.805	Fe I	4.283	-1.820
5837.700	Fe I	4.294	-2.337
5838.370	Fe I	3.943	-2.337
5844.917	Fe I	4.154	-2.940
5845.266	Fe I	5.033	-1.818
5849.682	Fe I	3.695	-2.993

TABLE 2—*Continued*

$\lambda(\AA)$	Species	χ(eV)	$\log gf$
5853.149	Fe I	1.485	-5.268
5856.083	Fe I	4.294	-1.640
5861.107	Fe I	4.283	-2.452
5000.743	Fe II	2.778	-4.745
5018.440	Fe II	2.891	-1.213
5132.669	Fe II	2.807	-4.000
5234.625	Fe II	3.221	-2.240
5264.812	Fe II	3.230	-3.188
5284.098	Fe II	2.891	-3.010
5325.559	Fe II	3.221	-3.170
5414.046	Fe II	3.221	-3.620
5425.247	Fe II	3.199	-3.210
5534.847	Fe II	3.244	-2.770

NOTE.—Adopted excitation potentials and gf-values for Fe I and Fe II lines

TABLE 3
EQUIVALENT-WIDTH MEASUREMENTS

λ	#1	#2	#3	#4	#5	#6	#7	#8	#9	#10
5307.361	132	109	185	117	118	154	154	165	116	135
5322.041	92	84	140	86	85	114	100	118	819	102
5497.516	...	183	...	172	...	...	...	...	...	...
5501.464	...	...	...	166	...	...	...	...	...	...
5522.447	...	50	...	47	...	73	...	...	...	...
5536.583	35	25	...	17	...	34	...	...	...	...
5539.284	42	...	54	23	32	45	45	44	28	...
5549.948	32	15	44	...	...	...	...	31	21	...
5559.638	18	...	19	...	...	...	15	11	...	...
5560.207	63	...	...	57	60	72	68	68	56	62
5577.031	...	...	22	...	...	...	...	...	15	...
5579.335	...	14	34	10	...	...	25	23	16	...
5607.664	...	...	44	...	25	...	35	33	...	27
5608.974	25	...	35	...	...	24	31	...	...	13
5611.361	31	...	37	14	19	...	37	27	...	19
5618.631	70	58	91	56	62	78	71	76	58	64
5619.224	21	11	195	6	10	15	21	15	...	...
5636.696	40	...	65	24	...	48	...	40	32	...
5638.262	98	78	126	78	89	99	92	98	77	96
5661.012	...	...	15	...	...	...	13	...	...	...
5677.684	20	...	24	...	15	17	24	20	...	...
5679.025	66	54	...	53	63	74	72	74	51	66
5696.103	27	17	...	...	...	22	...	...	18	18
5698.023	...	28	50	...	31	39	47	...	...	30
5705.466	50	48	88	44	54	63	65	...	47	52
5717.835	76	69	105	66	67	86	81	82	...	72
5724.454	19	...	19	...	...	...	...	...	14	9
5759.261	...	...	20	...	13	...	50	15	12	11
5760.345	44	...	65	29	41	53	23	...	38	36
5784.657	52	36	77	34	42	54	57	60	44	41
5793.913	51	38	71	39	46	55	54	57	42	...
5806.717	60	55	90	49	56	68	66	66	...	64
5807.782	27	...	41	16	23	26	39	30	17	...
5809.217	70	54	98	53	56	76	70	79	...	70
5811.917	...	15	35	...	...	...	29	25	16	...
5814.805	36	34	59	...	37	...	48	42	...	33
5837.700	...	13	...	12	16	...	28	21	...	...
5838.370	...	25	...	21	32	...	45	...	...	31
5844.917	...	...	...	...	...	...	16	...	8	8
5845.266	...	...	...	...	...	10	14	...	9	10
5849.682	...	14	31	...	17	20	30	26	19	14

TABLE 3—*Continued*

λ	#1	#2	#3	#4	#5	#6	#7	#8	#9	#10
5853.149	...	32	67	22	32	55	58	57	...	27
5856.083	51	...	70	...	42	51	53	56	39	...
5861.107	...	...	...	...	...	...	22.7	...	...	...
5000.743	...	...	...	...	...	...	...	...	...	...
5018.440	...	175	201	...	...	222	...	186	174	161
5132.669	39	...	37	41	35	49	45	...	...	25
5234.625	87	71	100	92	72	100	86	81	72	786
5264.812	45	43	55	54	44	57	56	44	38	42
5284.098	64	63	82	76	...	...	...	67	62	...
5325.559	...	42	54	56	47	57	56	45	...	36
5414.046	30	30	30	37	34	...	42	30	29	20
5425.247	46	41	52	57	46	61	51	44	38	38
5534.847	...	60	70	73	59	74	70	...	...	...

NOTE.—Equivalent widths of Fe I and Fe II lines (given in mÅ) for 10 stars. Stellar identifications are provided in Table 4.

TABLE 4

STELLAR PARAMETERS AND METALLICITIES DERIVED FROM CLASSICAL SPECTROSCOPIC ANALYSIS FOR 10 SELECTED STARS

Star	ID	T_{eff} (K)	*log g* (dex)	ξ (km/s)	[Fe/H] (dex)
G0858+00.192	#1	4630	2.2	1.1	-0.31 ±0.07
G0901+00.175	#2	4760	2.6	0.9	-0.48 ±0.06
G1007+00.5	#3	4490	2.5	1.8	-0.12 ±0.05
G1018-05.46	#4	4670	1.6	1.2	-0.77 ±0.05
G1030+00.15	#5	4780	2.6	0.9	-0.34 ±0.06
G1042-05.69	#6	4370	1.1	1.4	-0.63 ±0.06
G1053+00.4	#7	4400	1.2	0.9	-0.35 ±0.07
G1113+00.20	#8	4240	1.6	1.4	-0.56 ±0.06
G1147-05.31	#9	4600	2.1	0.6	-0.48 ±0.07
G1147-05.49	#10	4720	3.0	1.3	-0.41 ±0.08

NOTE.—Name of star, its ID in Table 3, effective temperature, surface gravity, microturbulent velocity, and [Fe/H].

TABLE 5
RV-VARIABILITY FOR THE 148 McDONALD REPEATED STARS

Name	M (mag)	$T_{\rm eff}$ (K)	D_{ph} (Kpc)	[Fe/H]$_{ph}$ (dex)	log g_{sp} (dex)	Δ log g_{sp} (dex)	[Fe/H]$_{sp}$ (dex)	Δ [Fe/H]$_{sp}$ (dex)	σ (km/s)	N
G0118-05.38	11.97	4814	0.9	-1.0	3.13	0.13	0.00	0.05	0.165	2
G0131+00.86	11.55	4707	0.9	-1.2	2.34	0.17	-0.80	0.14	0.919	2
G0142+05.56	10.91	3959	2.2	-0.9	1.20	0.65	-0.60	0.28	0.489	2
G0142+05.70	12.27	4196	2.3	-0.6	1.93	0.25	-0.67	0.25	0.287	2
G0151+00.72	11.29	4334	1.7	-0.6	2.34	0.06	-0.07	0.22	0.287	3
...										

NOTE.—Name of star, Washington M magnitude (which is approximately Johnson's V), effective temperature, photometric distance, photometric metallicity [Fe/H], spectroscopic surface gravity log g and its accuracy, spectroscopic metallicity [Fe/H] and its accuracy, RV variability, and number of RV-observations for the northern sample objects.
The full version of the Table is presented in electronic form.

TABLE 6
RV-VARIABILITY FOR THE 341 CORALIE REPEAT OBSERVATION STARS

Name	M (mag)	T_{eff} (K)	D_{ph} (Kpc)	[Fe/H]$_{ph}$ (dex)	σ (km/s)	N
G0000-56.81	11.92	4066	3.5	-1.1	0.004	3
G0012-28.38	11.71	3891	3.8	-1.0	0.182	3
G0016-39.1207	11.46	4418	4.3	-2.0	1.104	7
G0016-39.2075	11.93	4580	1.7	-1.0	0.635	2
G0016-39.3290	11.41	4753	0.8	-0.7	2.060	4
...						

NOTE.—Name of star, Washington M magnitude, effective temperature, photometric distance, photometric metallicity [Fe/H], RV variability, and number of RV observations for objects of the southern sample.
The full version of the Table is presented in electronic form.

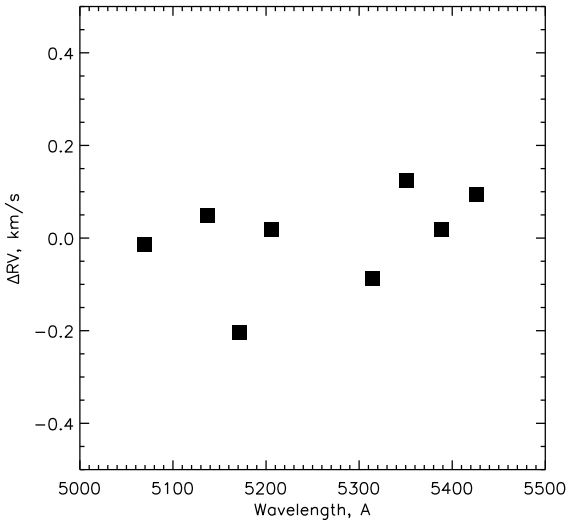

Fig. 1.— An example of the order-to-order radial velocity differences for the program star G1113+00.20. The wavelength corresponds to the middle of each respective order.

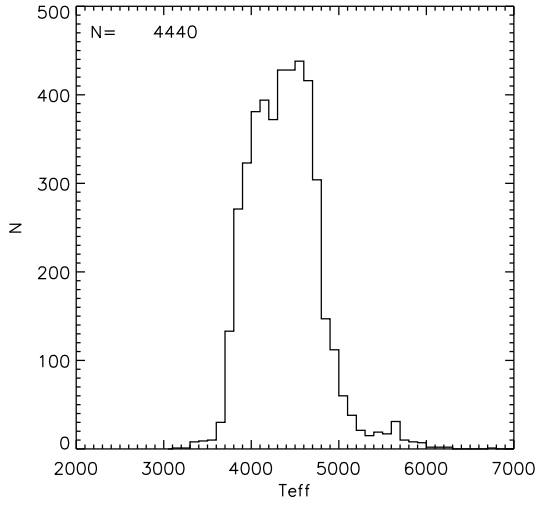

Fig. 2.— Distribution of T_{eff} for the general sample of 4440 GGSS candidates.

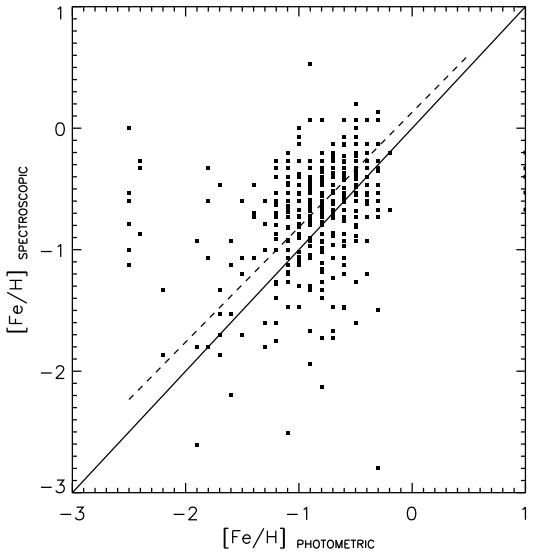

Fig. 3.— The comparison of metallicities estimated from high-resolution spectroscopy (see text) and "photometric" [Fe/H] (Rhee et al. 2001). The dashed line shows the "robust" least absolute deviation fit to the data. The values of [Fe/H] for most of the stars with intermediate metallicity approximately follow a linear relation with dispersion of order 0.4 dex. The spectroscopic [Fe/H] is systematically higher than the photometric one by about 0.16 dex.

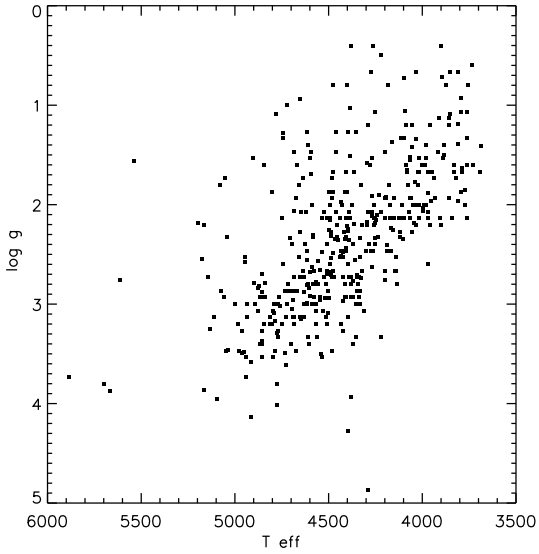

Fig. 4.— The relation between surface gravity and effective temperature for 434 stars from our northern sample.

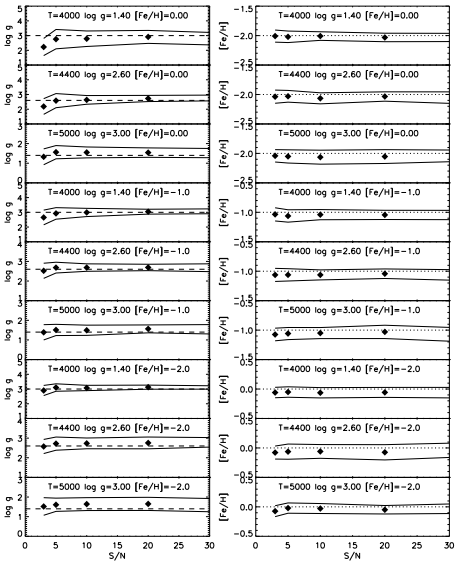

Fig. 5.— The 1-sigma level scatter of estimated stellar atmospheric parameters (*solid curves*) as a function of S/N. The mean values of log g and [Fe/H] found for one hundred deteriorated model spectra are designated by the diamonds. The dashed lines represents the initial (true) parameters (log g or [Fe/H]) of the model spectra. The results of simulations are shown for models typical of the GGSS red giants: T_{eff} = 4000, log $g = 1.4$, $T_{eff} = 4400$, log $g = 2.6$, and T_{eff} = 5000, log g = 3.0, and for metallicities [Fe/H]=0, -1, and -2.

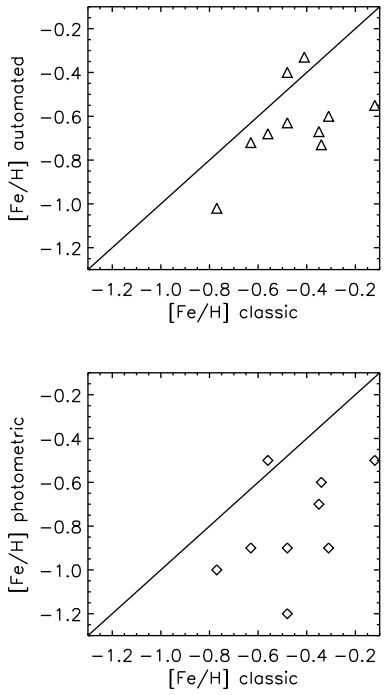

Fig. 6.— Metallicities for 10 GGSS stars measured three different ways: using Washington photometry, the automated method, and a detailed spectroscopic analysis. The three methods show general agreement.

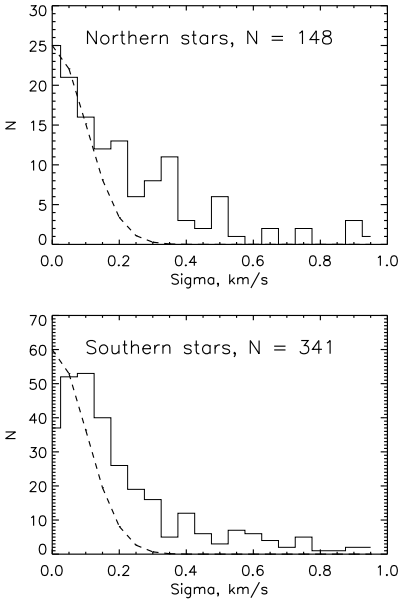

Fig. 7.— Distribution of the variation of radial velocity, σ (in km s^{-1}) for the northern (upper panel) and southern (lower panel) subsamples (148 and 341 stars, respectively) with two or more estimates of RV. The dashed line shows a gaussian distribution with 100 m s^{-1} sigma).

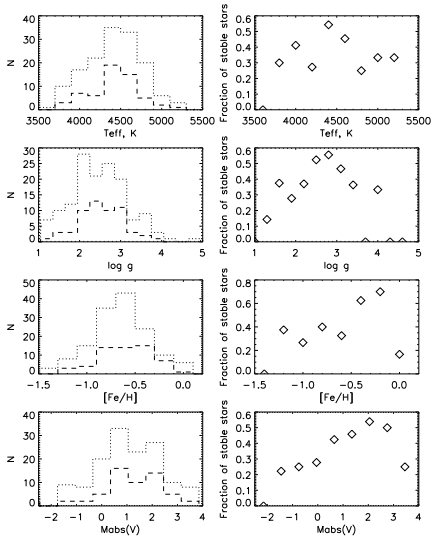

Fig. 8.— Left panels: histograms of distribution of T_{eff}, $log\ g$, [Fe/H], and M_V for the stars whose $\sigma < 100$ m s^{-1} (dashed line) in comparison with the whole sample (dotted line). The right side panels show the corresponding fraction of stable stars in bins of the histogram.

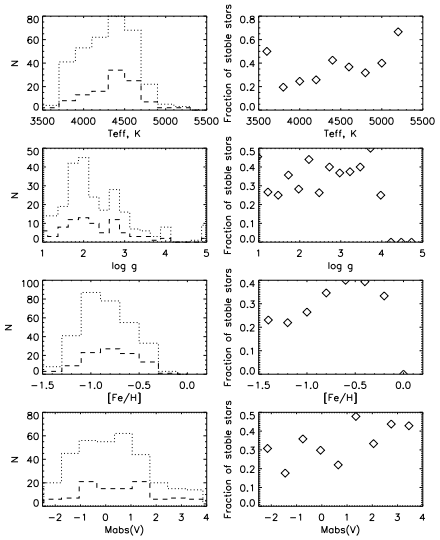

Fig. 9.— The same as in Figure 9, but for the southern subsample.

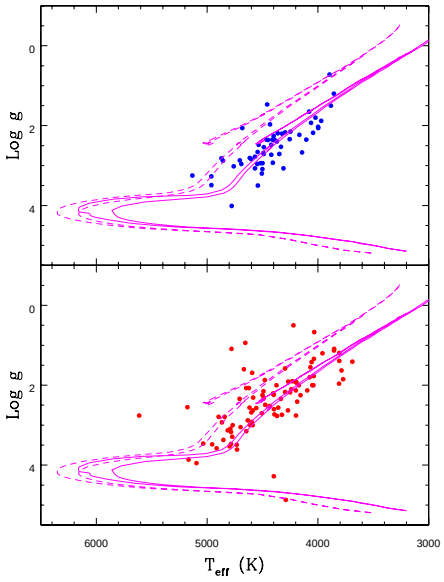

Fig. 10.— The spectroscopically derived surface gravity, log g, plotted versus $T_{\rm eff}$ for the McDonald northern sample: The top panel shows stars with $\sigma < 100$ m s^{-1} while the bottom panel shows those with RV-variability greater than 100 m s^{-1}. The RV-stable stars are more concentrated in the log g – T_{eff} plane than the variables. The continuous curves are isochrones from Girardi et al. (2000), with the dashed curves having [Fe/H]=-0.7 and the solid curves [Fe/H]=0.0. The two isochrones for each metallicity have different ages of 3.5 Gyr and 8.9 Gyr, respectively. The concentrated "clump" of RV-stable stars may correspond to the core-He burning red giant phase of stellar evolution.

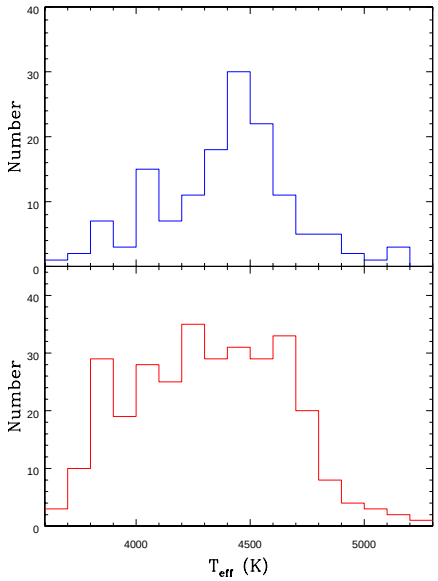

Fig. 11.— Effective temperature histograms segregated as the RV-stable stars (top panel) and RV-variable stars (bottom panel) for the combined northern and southern data sets. The RV-stable stars are sharply peaked near T_{eff}=4500±200K, while the RV-variable stars are more spread out in temperature. This provides additional support for the suggestion that the core-He burning stars, with only mild metal deficiencies, may be intrinsically more stable in radial velocity.